

Chapter 8

Models of Venus Atmosphere

**Sebastien Lebonnois, Christopher Lee, Masaru Yamamoto,
Jonathan Dawson, Stephen R. Lewis, Joao Mendonca, Peter Read,
Helen F. Parish, Gerald Schubert, Lennart Bengtsson, David Grinspoon,
Sanjay S. Limaye, Hauke Schmidt, Håkan Svedhem, and Dimitri V. Titov**

In the context of an International Space Science Institute (ISSI) working group, we have conducted a project to compare the most recent General Circulation Models (GCMs) of the Venus atmospheric circulation. A common configuration has been decided, with simple physical parametrization for the solar forcing and the

S. Lebonnois (✉)

Laboratoire de Meteorologie Dynamique, CNRS, Jussieu, Box 99, 75252 Paris, France
e-mail: Sebastien.Lebonnois@lmd.jussieu.fr

C. Lee

Ashima Research, 600 S. Lake Ave, Pasadena, CA 91106, USA
e-mail: lee@ashimaresearch.com

M. Yamamoto

Institute for Applied Mechanics, Kyushu University, 6-1 Kasuga-kouen, 816-8580, Kasuga, Japan
e-mail: yamakatu@riam.kyushu-u.ac.jp

J. Dawson • S.R. Lewis

Department of Physics and Astronomy, The Open University, Walton Hall,
Milton Keynes, MK7 6AA, UK
e-mail: jon.dawson@open.ac.uk

Planetary and Space Science Institute, Open University, Walton Hall,
Milton Keynes, MK7 6AA, UK
S.R.Lewis@open.ac.uk

J. Mendonca • P. Read

Department of Physics, Oxford University, Clarendon Laboratory, Parks Road,
Oxford, OX1 3PU, UK
e-mail: mendonca@atm.ox.ac.uk

Atmospheric, Oceanic and Planetary Physics, University of Oxford, Clarendon Laboratory,
Parks Road, Oxford, OX1 3PU, UK
e-mail: p.read1@physics.ox.ac.uk

H.F. Parish • G. Schubert

Department of Earth and Space Sciences, University of California Los Angeles, 595 Charles
Young Drive East, Los Angeles, CA 90095-1567, USA
e-mail: hparish@ess.ucla.edu; schubert@ucla.edu

boundary layer scheme. Six models have been used in this intercomparison project. The nominal simulation was run for more than 200 Venus days, and additional sensitivity runs have been done by several models to test the trends visible in these models when parameters are varied: topography, upper and lower boundary conditions, horizontal and vertical resolution, initial conditions. The results show that even in very similar modeling conditions, the wind speeds obtained with the different GCMs are widely different. Super-rotation is obtained, but the shape (with or without marked high-latitude jets) and amplitude of the maximum zonal wind jet is different from one model to the other, from 15 to 50 m/s. Minor sensitivity is seen in several models to the upper boundary conditions, the topography or the vertical grid. Horizontal resolution and lower boundary conditions induce variations that are significant, affecting the amplitude and shape of the region of maximum zonal wind. Two models were started from an atmosphere already in super-rotation. The simulations did not converge back to the nominal simulations, maintaining maximum zonal winds over 70 m/s (and even 100 m/s) without marked high-latitude jets. This study shows how sensitive GCMs are to the weak forcing of Venus atmosphere, and how difficult it is to draw precise conclusions on the circulation obtained with a single model, as well as on its sensitivity to some parameters.

L. Bengtsson

International Space Science Institute (ISSI), Hallerstrasse 6, 3012 Bern, Switzerland

email:Bengtsson@issibern.ch

D. Grinspoon

Department of Space Science, Denver Museum of Nature and Science,
2001 Colorado Blvd., Denver, CO 80205, USA

email:dgrinspoon@dmns.org

S.S. Limaye

Space Science Engineering Center, University of Wisconsin, 1225 West Dayton Street,
Madison, WI 53706, USA

email:SanjayL@ssec.wisc.edu

H. Schmidt

Atmosphäre im Erdsystem, Max-Planck-Institut für Meteorologie, Bundestrasse 53,
D-20146, Hamburg, Germany

email:hauke.schmidt@zmaw.de

H. Svedhem • D.V. Titov

ESA/ESTEC, Keplerlaan 1, PO Box 299, 2200 AG, Noordwijk, The Netherlands

email:hsvedhem@rssd.esa.int

ESTEC/ESA, Postbus 299, NL-2200, AG Noordwijk, The Netherlands

email:dmitri.titov@esa.int

8.1 Introduction

With the success of the European Venus Express mission, Venus' atmosphere has been put once more under the lights of international research. Many groups around the world are analyzing observational datasets, from space and ground-based campaigns. To support and complement these analyses modeling of the atmosphere of Venus is needed. The state of worldwide research in this field, as well as the links with the modeling of the Earth's atmosphere, have been the purpose of the ISSI working group producing the present book. In this context, several specialists in the modeling of Venus' and Earth's atmospheres came together, and decided to assess current models of the Venusian atmosphere through an intercomparison project, based on available models, though limited to models that use a simplified thermal forcing.

Starting with the pioneering work of [Young and Pollack \(1977\)](#) more than thirty years ago, the modeling of the circulation of Venus' atmosphere has always been a challenge. Most of the General Circulation Models (GCMs) developed for Venus have been adapted from Earth GCMs. Recently published models include [Yamamoto and Takahashi \(2003a, 2004, 2006, 2009\)](#); [Takagi and Matsuda \(2007\)](#); [Dowling et al. \(2006\)](#); [Hollingsworth et al. \(2007\)](#); [Lee \(2006\)](#); [Lee et al. \(2005\)](#); [Lee et al. \(2007\)](#); [Herrnstein and Dowling \(2007\)](#); [Kido and Wakata \(2008\)](#); [Lee and Richardson \(2010\)](#); [Lebonnois et al. \(2010\)](#); [Parish et al. \(2011\)](#). These models have used simplified physical and radiative parameterizations. Only [Lebonnois et al. \(2010\)](#) used a complete radiative transfer model to compute the temperature field self-consistently. The results presented in these different models vary widely, and may even be contradictory in some aspects.

The idea of comparing the results of different models forced with the same physical parameters is not new. In the case of Venus, it was recently done using numerical experiments with three different dynamical cores [Lee and Richardson \(2010\)](#). We decided to build upon this first work by extending the comparison to five additional models. The models included in this study are:

- **CCSR**—Kyushu/Tokyo CCSR/NIES GCM (simplified forcing version): Masaru Yamamoto ([Yamamoto and Takahashi 2003b, 2004, 2006](#)).
- **LMD**—Paris LMD GCM: Sebastien Lebonnois ([Lebonnois et al. 2010](#)), in a simplified radiative forcing configuration.
- **OU**—Open University spectral GCM: Jonathan Dawson, Stephen Lewis.
- **UCLA**—UCLA/LLNL Aerospace CAM GCM: Gerald Schubert, Curt Covey, Helen Parish, Richard Walterscheid ([Parish et al. 2011](#)). This model had to be run in a very high resolution configuration (approximately $1^\circ \times 1^\circ$) due to numerical dissipation issues.
- **OX**—Oxford GCM: Joao Mendonca, Peter Read. Simulations done by Christopher Lee during his PhD thesis have also been used ([Lee et al. 2005](#); [Lee 2006](#); [Lee et al. 2007](#)).

- **LR10**—GFDL FMS GCM: Christopher Lee (Lee and Richardson 2010). The simulations were run before this work, using three different dynamical cores.

The indicated acronyms will be used throughout this text to identify the simulations.

8.2 Intercomparison Protocol

The goal of this study is to build upon the intercomparison of Lee and Richardson (2010) where different GCMs, or different numerical cores, are forced with similar physical parameterizations to test the sensitivity of the simulated atmospheric circulation to the choice of numerical model.

To reach this goal, we have built a common protocol that the different teams involved in the project would have to follow to run a set of simulations, that would be compared together. The first simulation is designed to compare the behavior of the different dynamical cores. Then sensitivity simulations are run to see the sensitivity to several parameters in each model, and check the consistency of these sensitivities among the models.

8.2.1 Dynamical Cores

The set of models includes three different types of dynamical core implementations: three spectral models, three models based on finite differences schemes and two models based on finite volume discretization. The horizontal resolution was chosen close to $5^\circ \times 5^\circ$: 64×32 for grid models (72×36 for OX), T21 for spectral models. The UCLA model had to run at much higher resolution (approximately $1^\circ \times 1^\circ$) due to numerical dissipation issues. This makes direct comparison to other base simulations quite difficult, especially considering the impact of horizontal dissipation, as it will be shown below. However, we will include this simulation in the baseline run discussion. The vertical resolution has been equalized for the protocol, though several models also made some simulations with their usual vertical grid. The common vertical grid used is the one from Lebonnois et al. (2010), based on 50 levels. The OX and LR10 simulations were done only with a 32-level grid given in Lee et al. (2007).

All planetary parameters (e.g., gravity, planetary radius, rotation rate) are fixed to identical values (see e.g., Lee et al. 2007; Lebonnois et al. 2010). The specific heat is taken as constant, $C_p = 900$ J/kg/K. The reference simulations do not include topography. The atmosphere was taken at rest as initial condition, and simulations were run for a couple of hundred Venus days (from 187 Vdays for LR10 up to 600 Vdays for UCLA). One Vday is 117 Earth days, or approximately one third of an Earth year.

The horizontal dissipation scheme is usually deeply embedded in the dynamical cores, and is not a parameter that is easily modified. We left all the different implementations as they were in each dynamical core, though this dissipation was kept as low as possible in each model. The type of horizontal dissipation and typical parameter values used in the different models are listed in Table 8.1.

8.2.2 Common Physical Parameterization

8.2.2.1 Thermal Forcing

All models have been run using the same simplified scheme taken from Lee (2006). The radiative tendency (temporal variation between two model timesteps) on temperature at longitude λ , latitude ϕ and pressure level p is given by

$$\frac{\delta T_{\text{rad}}(\lambda, \phi, p, t)}{\delta t} = -\frac{T(\lambda, \phi, p, t) - T_0(\phi, p)}{\tau}, \quad (8.1)$$

where $T_0(\phi, p)$ is the forcing thermal structure, and τ is the time constant of this forcing. $T_0(\phi, p)$ and τ are taken from Lee (2006)

$$T_0(\phi, p) = T_{\text{ref}}(p) + T_1(p)(\cos(\phi) - C), \quad (8.2)$$

where $T_{\text{ref}}(p)$ is a reference temperature profile Seiff et al. (VIRA model, 1985), and $T_1(p)$ is a perturbation term giving the peak equator-to-pole difference. The constant C is the integral of $\cos \phi$ over the domain ($C = \pi/4$). The profile of $T_1(p)$ was chosen to reflect the peak in absorption of solar insolation within the cloud deck Lee (2006). The value of τ is 25 Earth days, decreasing slightly in the uppermost levels. In this formulation the diurnal cycle is not taken into account.

8.2.2.2 Upper Boundary Conditions

A sponge layer is included in the top four layers of the GCM. In the baseline simulations, this sponge layer includes Rayleigh friction damping horizontal winds to zero. Time constants are $\eta \times 10^6 \approx$ Earth days for the LR10 models. For the other models, these time constants were fixed to 9.6×10^4 s (1.12 Earth days) for the top layer, then 1.20×10^5 , 1.23×10^5 , and 1.60×10^5 s for the next three layers, following values used in Newman and Leovy (1992). These values are roughly half the values used in the LR10 models and therefore apply a stronger damping at the model top.

For the OX simulation, this damping is applied only to the eddy components of the horizontal wind speed. The other models have adopted this configuration as a sensitivity test (see below). However, we have included the OX simulation in the basic comparison, since the influence of this parameter is small and limited to upper levels (this is discussed below).

Table 8.1 Summary of common and distinct parameters in the GCMs used for this work

Models	CCSR	LMD	OU	UCLA	OX	LR10
Dynamical core ^a	S	FD	S	FV	FD	S, FD, FV
Horizontal resolution	T21	64 × 32	T21	360x180	72x37	T21, 64x32
Duration of the simulations (Vdays)	250	250-350	500	600	222	187-300
Vertical grid	50 levels	50 levels	50 levels	50 levels	32 levels	32 levels
Horizontal dissipation	6th order	squared Lapl.	Del-8	Del-squared	6th order	8th order (S) 4th order (FD)
Time constant	3 Edays	2×10^4 s	4.3×10^4 s	2.2×10^4 s	30 Edays	div. damping (FV) 3 Edays (S,FD) 1 Eday (FV)
Vertical eddy coefficient, K	$0.15 \text{ m}^2 \text{ s}^{-1}$	$0.15 \text{ m}^2 \text{ s}^{-1}$	$0.15 \text{ m}^2 \text{ s}^{-1}$	$0.15 \text{ m}^2 \text{ s}^{-1}$	None	None
Thermal forcing	All models: From Lee (2006)					
Sponge layer	All models: 3 layers					
Surface friction	All models: Rayleigh friction, 1 layer					

^aS = “spectral” model, FD = “finite differences” and FV = “finite volumes”.

Table 8.2 Summary of the simulations done by the different groups

Simulations		CCSR	LMD	OU	UCLA	OX	LR10
base	Baseline	X	X	X			XXX
topo	Topography	X	(X) ^a	X			
spgl	Sponge layer (only eddies)	X	X	X		X	XXX
pbl[n]	Different PBL	X	XX				
lres	Low horizontal resolution	X	X	X			
hres	High horizontal resolution	X	X	X	X		
vgrd	Different vertical grid	X		XX			
uini	Different initial state	X	X				

^aParenthesis indicate: for LMD, simulation run before this work (Lebonnois et al. 2010); for OX, simulations run during C. Lee's PhD (Lee 2006)

8.2.2.3 Surface Friction and Vertical Eddy Diffusion

The most simple surface boundary layer is used in the baseline simulation: a Rayleigh friction in the first layer of the model with a time constant fixed to 3 days, together with a constant vertical dissipation coefficient, $k_v = 0.15 \text{ m}^2 \text{ s}^{-1}$. For the LR10 simulations, done before this protocol was agreed upon, the Rayleigh friction time constant is fixed to 25 days, and no explicit vertical dissipation is taken into account in the models. Similarly, for the OX simulation, a Rayleigh friction time constant of 32 days is used as well as no explicit vertical dissipation.

Every model kept its own implementation for the temperatures in the soil. For example, in the LMD GCM, a soil model with 11 layers is used.

8.2.3 Sensitivity Simulations

Some sensitivity studies of different parameters could only be done by some of the models. These different simulations are summarized in Table 8.2 and will be discussed in Sect. 8.3.4 of Chap. 7.

8.2.3.1 Topography (topo)

The CCSR and OU models have been run with topography. For the LMD model, the baseline simulation could not be run with topography, due to unsolved instability problems. However, one simulation in Lebonnois et al. (2010) included topography, though the lower boundary conditions are different from the baseline run (see below).

8.2.3.2 Upper Boundary Conditions (spgl)

As was done in the LR10 and OX simulations, we also tried to damp only the eddy terms in the horizontal winds within the sponge layer.

8.2.3.3 Lower Boundary Layer Scheme and Vertical Eddy Diffusion Coefficient (pbl)

For the LMD GCM, two other parameterizations have been used to test the impact of the lower boundary layer scheme and vertical eddy diffusion coefficient. The first one (*pbl2*) was used in [Lebonnois et al. \(2010\)](#), and is described in this paper. This parameterization computes the vertical diffusion flux, the surface drag, and the diffusion coefficient.

The second one (*pbl3*) is a “Mellor and Yamada” parameterization [Mellor and Yamada \(1982\)](#), taken from the Earth version of the LMD GCM. This parameterization is fully described in the Appendix B of [Hourdin et al. \(2002\)](#). The surface drag coefficient is computed as follow: $C_d = (0.4 / \ln(1 + z_1/z_0))^2$, where z_1 is the altitude of the center of the first layer, and z_0 is the roughness coefficient, taken equal to 1 cm.

For the CCSR GCM, a “bulk” parameterization has also been used (*pbl1*). We set the drag coefficient C_D to 4×10^{-3} for temperature and horizontal flow ([Del Genio et al. 1993](#)).

8.2.3.4 Horizontal Resolution (lres and hres)

For the CCSR, LMD and OU models, three different resolutions were used, to evaluate the impact of this parameter on the modeled circulations. The horizontal resolutions used are T10, T21 and T42 for the CCSR and OU spectral models, and 32×16 , 64×32 and 128×64 for the LMD finite difference model. The UCLA simulation, run at very high horizontal resolution, may also be discussed compared to the *hres* case.

8.2.3.5 Vertical Grid (vgrd)

The CCSR model was run both with its original vertical grid of 52 levels, and with the baseline 50-level grid from [Lebonnois et al. \(2010\)](#). The OX model has only been run with its original 32-level vertical grid. The OU model was also run with this 32-level vertical grid, and also with an increased vertical resolution (100 levels). For this model, the *vgrd* notation will apply to the 32-level run, while the 100-level run is noted *vgrd2*.

8.2.3.6 Different Initial State (*uini*)

The CCSR and LMD models have also been run starting from a zonal wind field already in super-rotation. This initial field was imposed analytically. The equatorial vertical profile is linear in altitude, from zero at the surface to 110 m s^{-1} at 70 km, then down to zero at 100 km. This profile is then multiplied by a linear latitudinal factor in both polar regions: from zero at the pole to 1 at 50° latitude.

The impact of the initial state has been studied with an Earth-like GCM with slow rotation rate (Del Genio and Zhou 1996). In this case, no differences were noted between both initial states (rest vs super-rotation). However, Kido and Wakata (2008) have recently published simulations of the Venus' atmosphere, and they also tested both initial states. In their results, both simulations do not reach the same state, with much stronger winds in the second experiment. As we will show below, this is also the case in the simulations done for this work.

8.2.4 Other Published Works

There are many other published works that may be included in the discussions, though the simulations are not done in the framework detailed here. These works have been described in detailed in the previous chapter.

8.3 Results

8.3.1 Spin-Up Phase and Total Angular Momentum

For most simulations, we decided to run for 250 Vdays, but some simulations were run for longer times to test the stability of the results. In all simulations (except UCLA), the circulation was stabilized after the initial run, though the total angular momentum in the atmosphere was sometimes still increasing slightly.

In Fig. 8.1, the evolution of the total atmospheric angular momentum is plotted for several simulations, normalized to the total angular momentum of the atmosphere rotating with the same speed as the solid surface below, i.e. with the zonal wind equal to zero everywhere, which is the initial state of all the simulations but *uini*. This variable is equal to the super-rotation index used by Del Genio and Zhou (1996), or to 1 plus the super-rotation factor defined by Read (1986). It is mostly sensitive to the deepest regions of the atmosphere, so differences in its evolution and final value are often an illustration of differences in the zonal wind field of the deep atmosphere. The base simulations have a non-dimensional total angular momentum of 2 to 6, with atmospheres in super-rotation. These differences of the total angular momentum are mostly caused by differences among the dynamical cores in atmospheric circulation of the deep atmosphere.

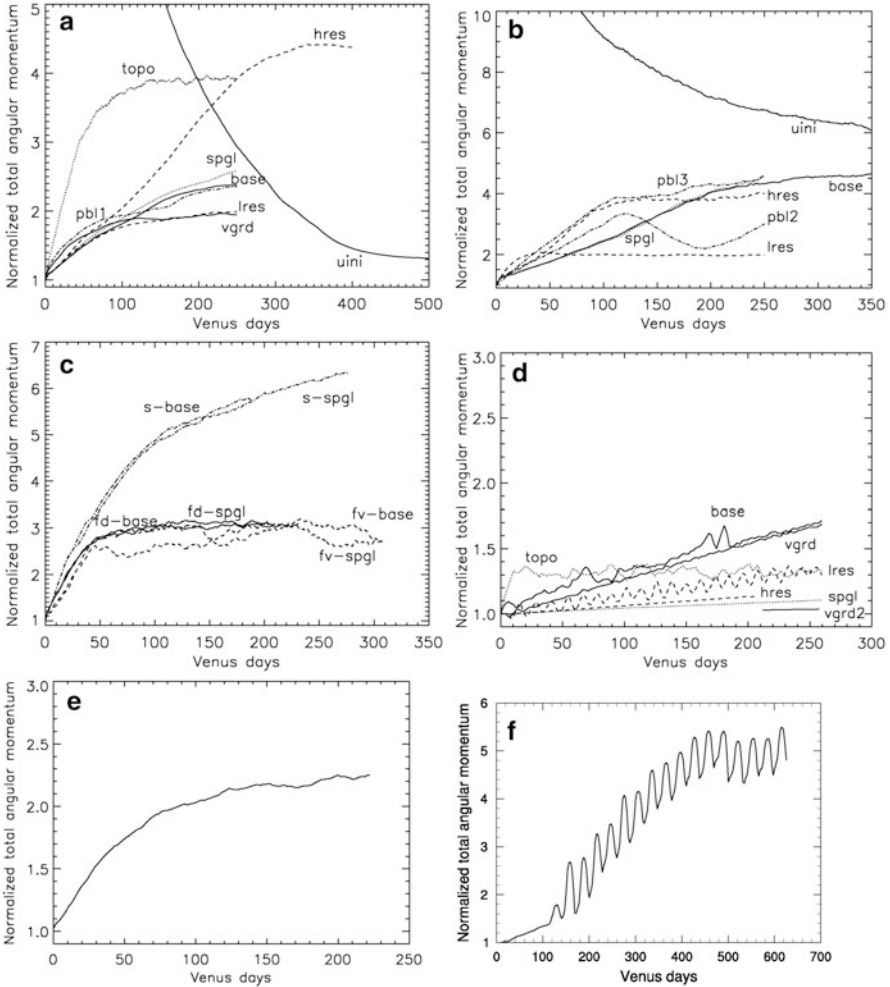


Fig. 8.1 Evolution of the total atmospheric angular momentum, normalized to its initial value (with atmosphere at rest), for all the simulations. (a) CCSR, (b) LMD, (c) LR10, (d) OU, (e) OX, (f) UCLA

The base simulations are almost the same as the *spgl* ones for all cases, which indicates that the total angular momentum is insensitive to the upper boundary parameterization. On the other hand, the sensitivities to the topography (*topo*), horizontal resolution (*lres*, *hres*), and initial condition (*uini*) are different among the models. These parameters strongly influence the angular momentum processes in the deep atmosphere. It is difficult to find any consistent trends in these temporal evolutions. However, the timescale for stabilization of the simulations are usually

between 100 and 200 Vdays, or even more. This illustrates that simulations of the Venus atmosphere need to be run for very long periods of time before they stabilize.

Two models show peculiar behaviors, the OU and UCLA models. In the OU models (Fig. 8.1d), the amplitude of the super-rotation stays very low compared to other models. The simulations appear to be far from equilibrium even after more than 200 Venus days, except for the *topo* simulation that is stabilized at a very low value (around 1.3). The oscillations seen in UCLA simulation (Fig. 8.1f) are due to large scale oscillations in the zonal wind distribution, particularly in the deep atmosphere, with a period of roughly ten Earth years as discussed in Parish et al. (2011). These oscillations are not seen in other models, though in the LMD-pbl2 simulation, some long-term variations are seen in the total angular momentum (Fig. 8.1b), that are due to oscillations at the cloud level between two different structures of the peak zonal winds. There are also small oscillations visible in the OU-lres simulation (Fig. 8.1d), though these don't affect the circulation much at the cloud level. Due to these oscillations, the UCLA results displayed in the next figures correspond to the average of the fields over a 10-year period.

8.3.2 Zonal Wind Field: Baseline Runs

The zonally averaged zonal wind fields obtained at the end of the simulations are displayed in Fig. 8.2. Temporal averaging is done over the last few Vdays of the simulations.

Super-rotation is obtained in the atmosphere in all the models, with maximum values in the cloud region and above, i.e., in the 10^5 – 10^3 Pa pressure range (roughly 50–75 km). Jets are predominantly visible at high latitudes, above 50° and are located somewhat deeper than the altitude of the peak equatorial super-rotation. Though this is the general pattern, wind fields are quite different from one model to the other. The jets are not visible in the CCSR and UCLA simulations (Fig. 8.2a and h). However, the UCLA wind field is a temporal average over the period of the oscillations Parish et al. (see 2011). In the LMD and OX simulations (Fig. 8.2b, d), the jets reach deeper into the atmosphere than in other simulations (the maximum peak is at 3×10^5 Pa for the LMD model). The amplitudes of the wind maxima are also significantly different from model to model. The strongest winds are obtained for the LR10-s simulation (Fig. 8.2e) with jets above 60 m/s while the average peak values are around 30–40 m/s. The vertical gradient and wind distribution in the deepest atmosphere (surface to 10^6 Pa) also vary from model to model. In many cases, the winds are still very small in this region and only develop above about 10^6 Pa level, while in other cases the vertical gradient in the zonal wind is already significant at the surface, with the high-latitude jet shape already visible there.

The nature of the dynamical core does not appear to play a crucial role. Though the two strongest zonal wind peaks are obtained with the CCSR and LR10-s spectral cores, it is not the case with the OU spectral core, in which zonal winds are the

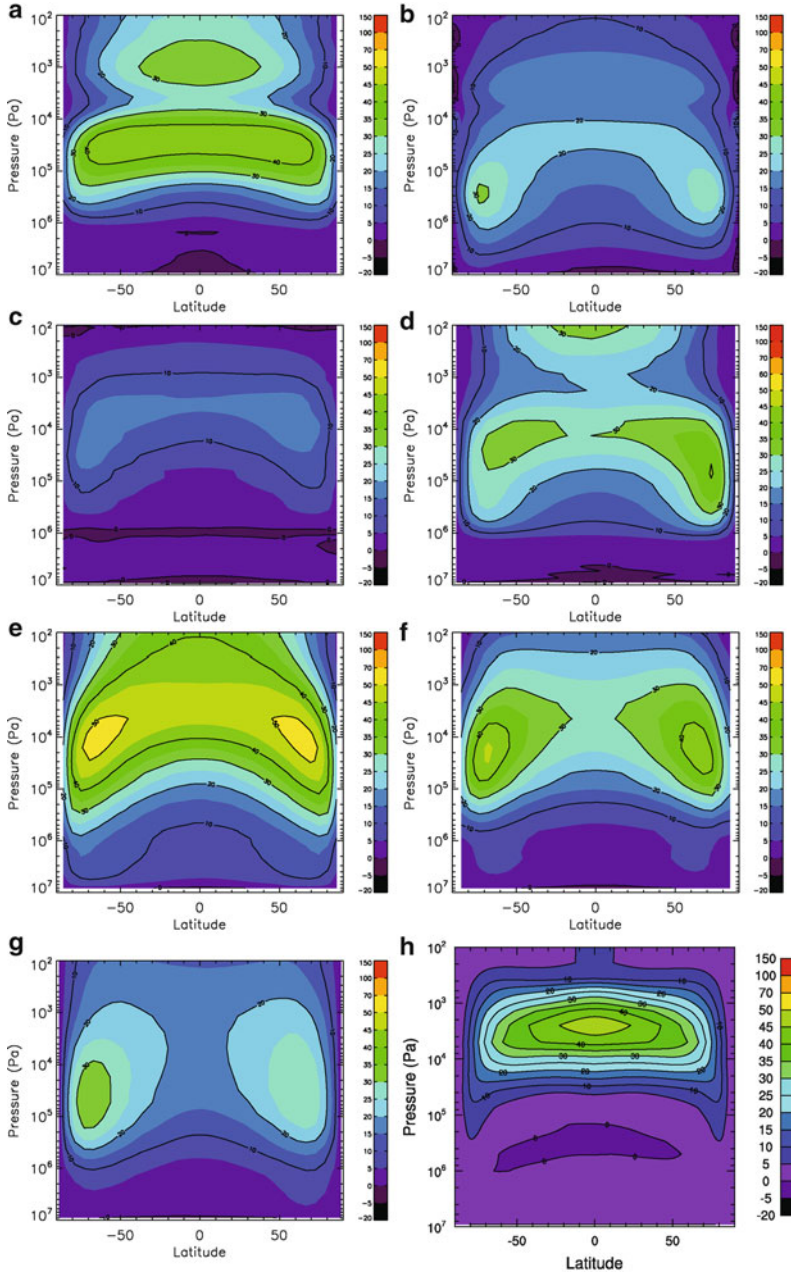


Fig. 8.2 Zonally and temporally averaged zonal wind fields obtained in all the baseline simulations. Unit is m/s. The first column is spectral models: (a) CCSR, (c) OU, (e) LR10-s. The second column is finite difference models: (b) LMD, (d) OX, (f) LR10-fd. The last line is finite volume models: (g) LR10-fv, (h) UCLA. For the UCLA simulation (h), the resolution is much higher than the other baseline runs and the results are averaged over a 10-year period. For the OX simulation, the sponge layer is applied to eddy terms only

weakest. The overall wind field shows many differences between the CCSR and LR10-s models, both in the cloud region and in the deepest part of the atmosphere.

Though the nature of two different dynamical cores may be the same (finite volume, A/B/C grid, spectral), the numerical implementation varies considerably between these models. Ranging from integration method (e.g., Euler vs. Runge-Kutta), to accuracy of the spatial differentiation (grid models), to Fourier filter properties (CFL based, resolution dependence, latitude dependence), these factors aren't equalized in the experiments. These variations probably contribute to the differences in a similar way as the nature of the core.

8.3.3 *Related Fields: Temperature Contrasts, Stream Functions*

The zonally and temporally averaged temperature contrasts shown in Fig. 8.3 are computed by subtracting the latitudinally averaged temperature field from the temperature field, for each pressure level. These contrasts are dominated by the same feature: cooler polar regions below a transition level corresponding to the zonal wind jet maxima, and warmer polar regions above. An additional inversion is located in the 10^3 – 10^4 Pa altitude region in the CCSR and LMD simulations. This may be related to the vertical discretization as seen in the *vgrd* simulation (see Sect. 8.3.4 of Chap. 7, Fig. 8.6). A similar inversion is seen close to the top of the OX model. However, it is a consequence of the different sponge layer used in the upper layers of the model. The amplitude of these contrasts are quite similar from model to model, though correlated with the peak zonal winds.

Figure 8.4 shows the zonally and temporally averaged stream function for the baseline simulations. The meridional circulation is dominated by large Hadley-type cells, from the surface up to the top of the models, with ascending air in the equatorial region and descending air over the polar regions. However, polar reverse cells are visible, clearly correlated to the poleward flank of the jets. These reverse cells are more or less visible depending on the model, and may reach the equatorial region in the upper atmosphere for some models (LMD, OX, LR10-s). The amplitude of the circulation in the deep atmosphere is quite similar among models.

8.3.4 *Sensitivities*

The sensitivity simulations show that many parameters have an impact on the zonal wind field. These effects may be small in some cases, much stronger in other cases. In this section, these effects will be discussed starting from the smallest impacts.

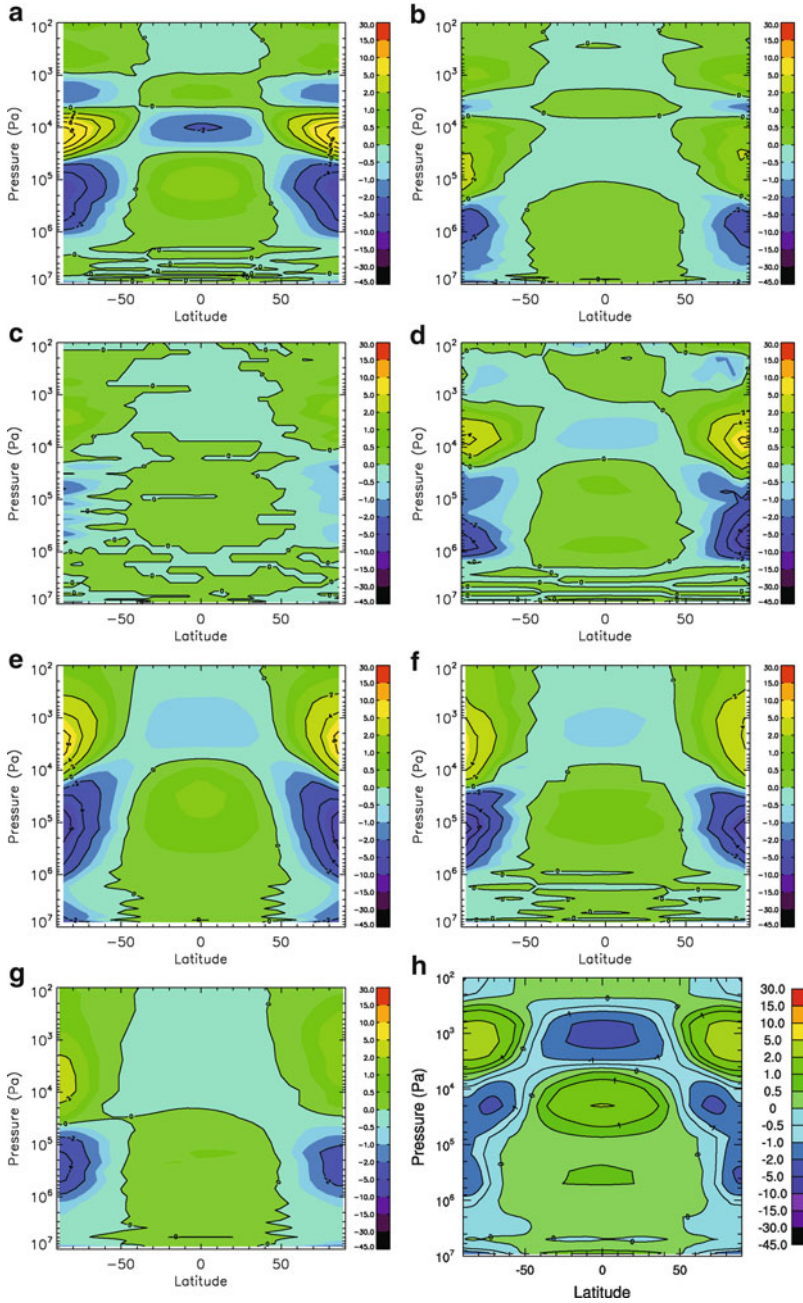


Fig. 8.3 Zonally and temporally averaged temperature contrasts obtained in all the baseline simulations. Unit is K. Models are the same as in Fig. 8.2

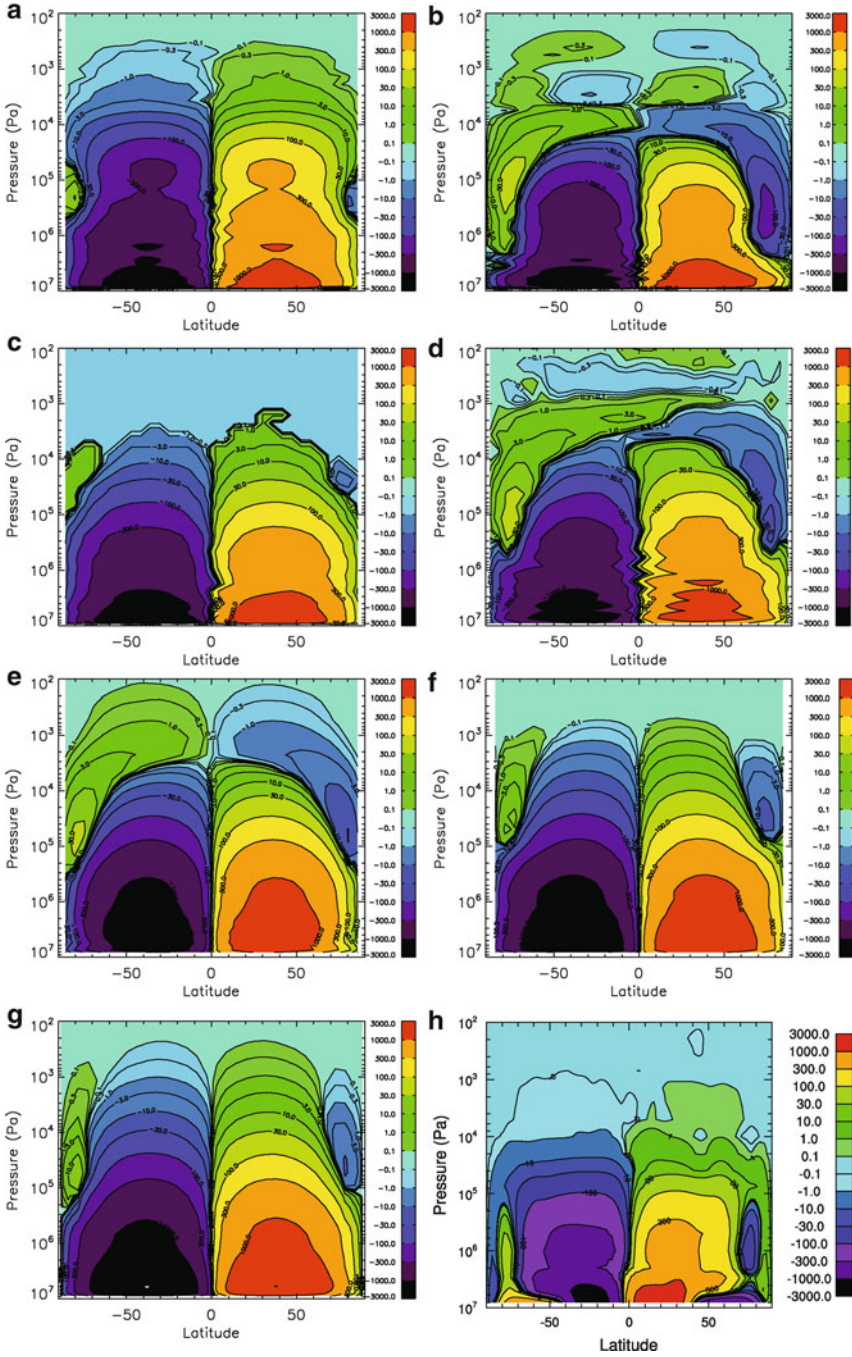


Fig. 8.4 Zonally and temporally averaged stream functions obtained in all the baseline simulations. Unit is 10^9 kg/s. Models are the same as in Fig. 8.2

8.3.4.1 Upper Boundary Conditions

When the upper boundary friction is modified (*spgl*), so that only the eddy part of the horizontal wind is damped in the sponge layer, the results are very similar to the *base* simulations. The corresponding zonal winds are shown in Fig. 8.5, to be compared to Fig. 8.2. For all the models, this change mainly affects the top layers, but not much below. There is not much effect in global budgets from damping the upper atmosphere to the mean, or to zero (Fig. 8.1). The amplitude of the jets is slightly affected (together with the pole-equator temperature contrast, not shown) but not in a consistent way among the different models, and without any correlation to model type. There is some effect on the lower layers because the thermal gradients are slightly modified and the characteristic vertical length scales of the features are larger than the damping region.

8.3.4.2 Vertical Grid

Different vertical grids have been used for the CCSR and OU models (*vgrd* simulations). The resulting fields are shown in Fig. 8.6. In the CCSR case, the feature previously located in the 10^3 – 10^4 Pa pressure range is not present anymore, suggesting that this feature is related to the distribution of the vertical levels. The shape of the zonal wind maximum has also been affected. In the OU model, the change from 50 to 32 vertical levels has also modified the zonal wind field, slightly reinforcing the jets, though their shape is not affected in the same way in both models. The stream function has also been influenced.

8.3.4.3 Topography

The effect of including Venusian topography in the CCSR and OU models is illustrated in Fig. 8.7. The effect may also be seen in the spin-up of the total angular momentum (Fig. 8.1), though this parameter mainly reflects how the use of topography affects the deepest layers of the atmosphere.

Herrnstein and Dowling (2007) reported a much faster spin up in the EPIC model with topography than without, with a resulting asymmetry between hemispheres because of Ishtar Terra. In the Oxford model used by Lee (2006) and Lee et al. (2007), an asymmetry was also found between hemispheres when including topography, but in the opposite sense to the EPIC model. Though the angular momentum had increased compared to the flat-planet case, no significant change was seen in the zonal wind at altitude or in the spinup speed of the model. In Lebonnois et al. (2010), experiments done with simplified radiative forcing are reported, with and without topography. In these experiments, including topography increases the amplitude of the jets, the total angular momentum, and the spinup speed.

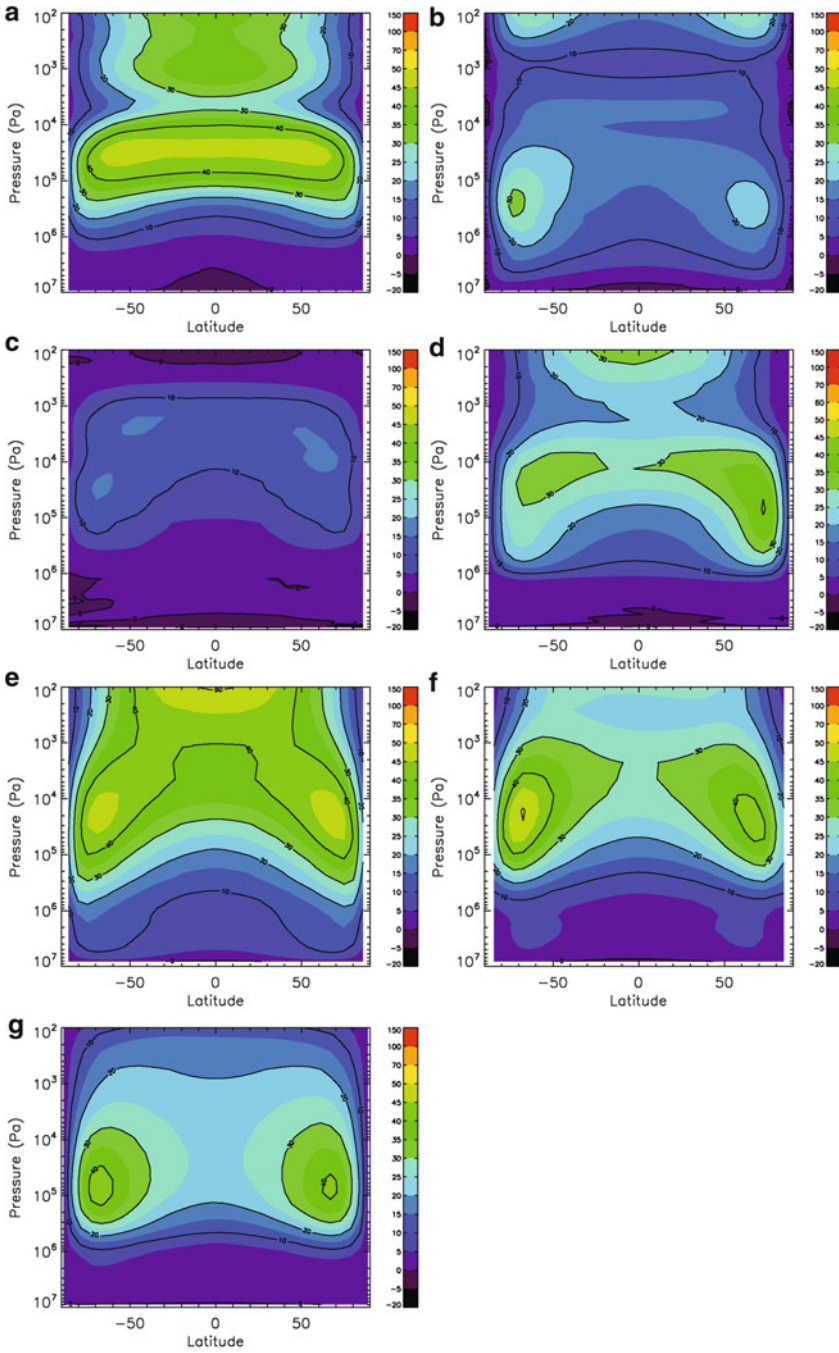


Fig. 8.5 Zonally and temporally averaged zonal wind fields obtained in the simulations with the eddies-only sponge layer *spl*. For the OX simulation (d), Fig. 8.2d is repeated. Models are placed the same way as in Fig. 8.2

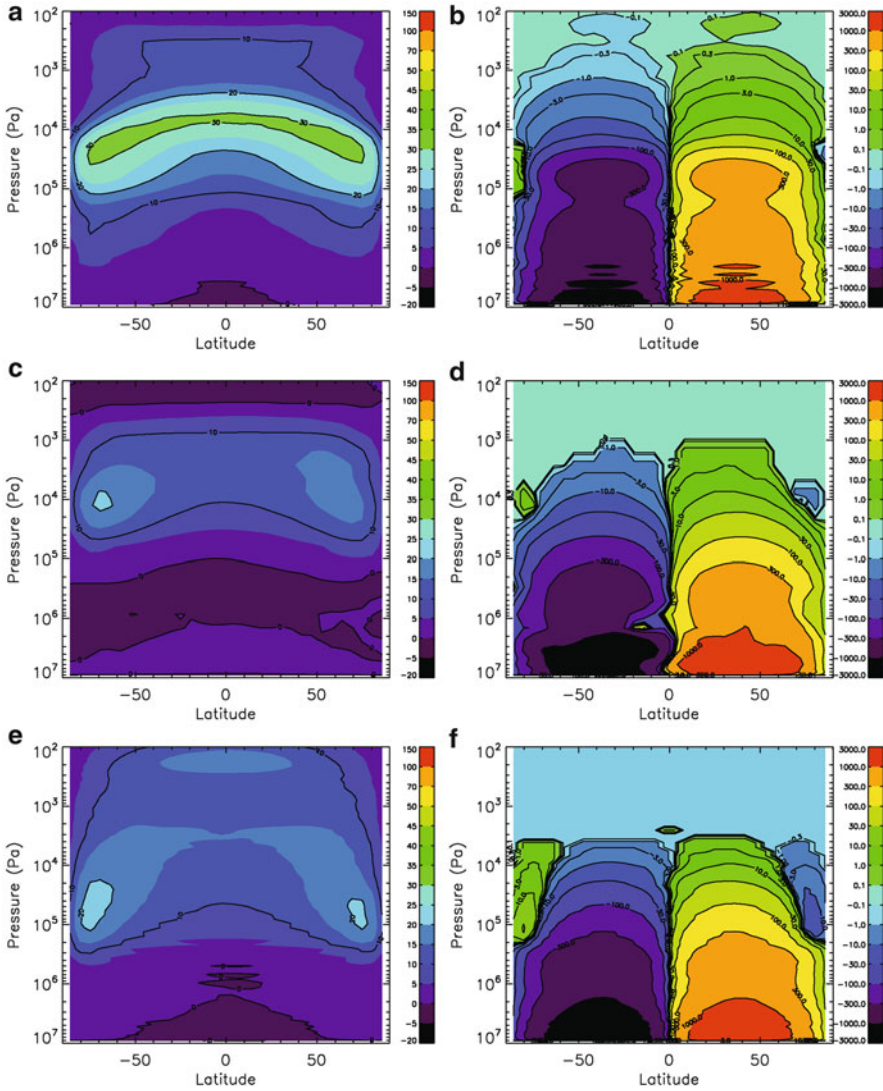


Fig. 8.6 Zonally and temporally averaged zonal wind and stream function obtained with the modified vertical grid (*vgrd*): (a, b) CCSR model; OU model (c, d) 32-level run and (e, f) 100-level run

In the two experiments done with topography for this intercomparison work, the effects on the amplitude of the jets are quite different: in the case of the CCSR model, increased angular momentum is obtained in the deep atmosphere but no effect is visible on the jets, while for the OU model, reduced jets are obtained and the angular momentum in the deep atmosphere decreases.

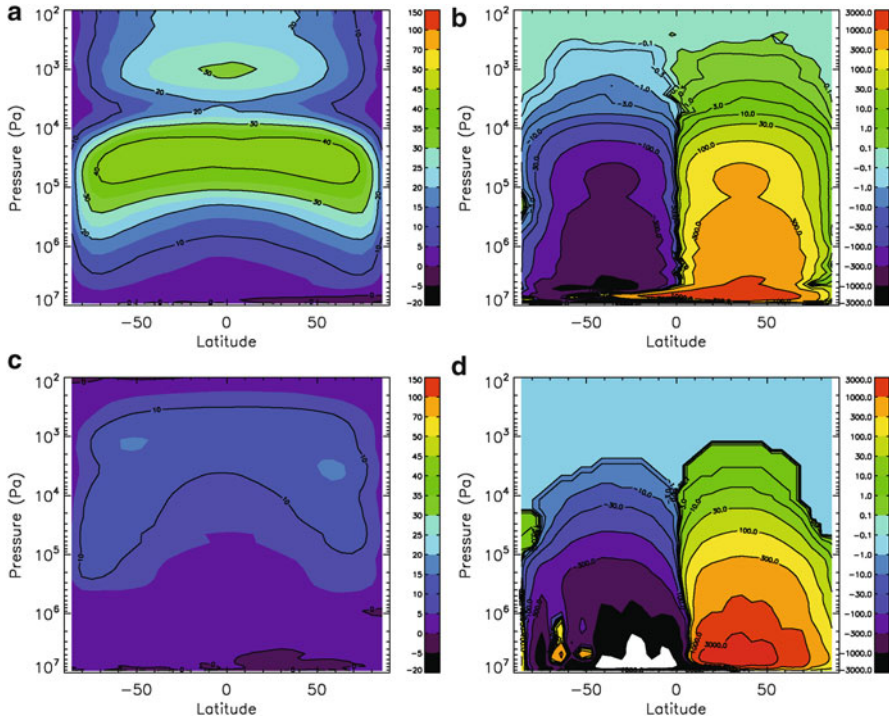


Fig. 8.7 Zonally and temporally averaged zonal wind and stream function obtained with topography (*topo*): (a, b) CCSR model, (c, d) OU model

Based on all these experiments, and their widely varied results, it is therefore very difficult to extract robust conclusions concerning the impact of the topography on numerical simulations of the Venus' atmosphere.

8.3.4.4 Lower Boundary Conditions

The sensitivity to lower boundary layer parameters and the vertical diffusion coefficient has been evaluated with two models, using alternative parameters: the effect may be quite strong in the deep atmosphere, influencing the angular momentum budget (and spin-up phase), and therefore the whole wind field.

In the CCSR-pb11 simulation, not much effect is seen compared to the baseline case. This conclusion has also been obtained in the Ph.D. work of Lee (2006), using a (Monin and Obukhov 1954) scheme with a similar roughness length of 3 cm. However, the LMD-pb12 simulation, with a quite different boundary layer parametrization shows some fluctuations in the wind field over timescales of more than a hundred Venus days, fluctuations especially present in the equatorial wind field within the cloud layer. The results of the LMD-pb13 simulation, with again a different boundary layer scheme, are very different from the others, with a large

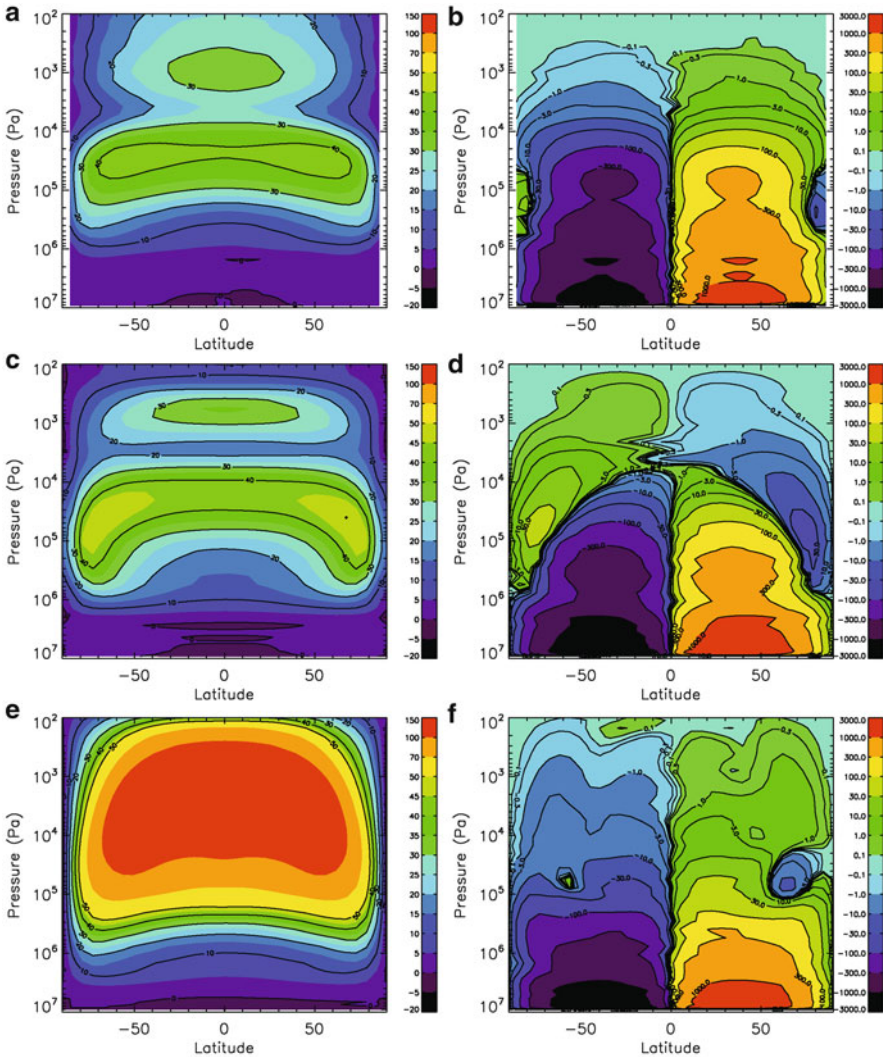


Fig. 8.8 Zonally and temporally averaged zonal winds and stream functions obtained in the simulations using different boundary layers: (a, b) CCSR-pb11, (c, d) LMD-pb12, (e, f) LMD-pb13

impact on the zonal wind field. A large super-rotation is produced, with very high zonal winds in the cloud region, almost uniform from equator to high latitudes. This is one of the most realistic simulations of Venus' circulation obtained with a simplified radiative forcing. It should be noticed from Fig. 8.1b that this simulation has a very similar total angular momentum to the baseline simulation, illustrating the fact that this variable is mostly reflecting the deep atmosphere. It would be interesting to test this more complex boundary layer scheme on other models, to see whether this strong impact is robust or not (Fig. 8.8).

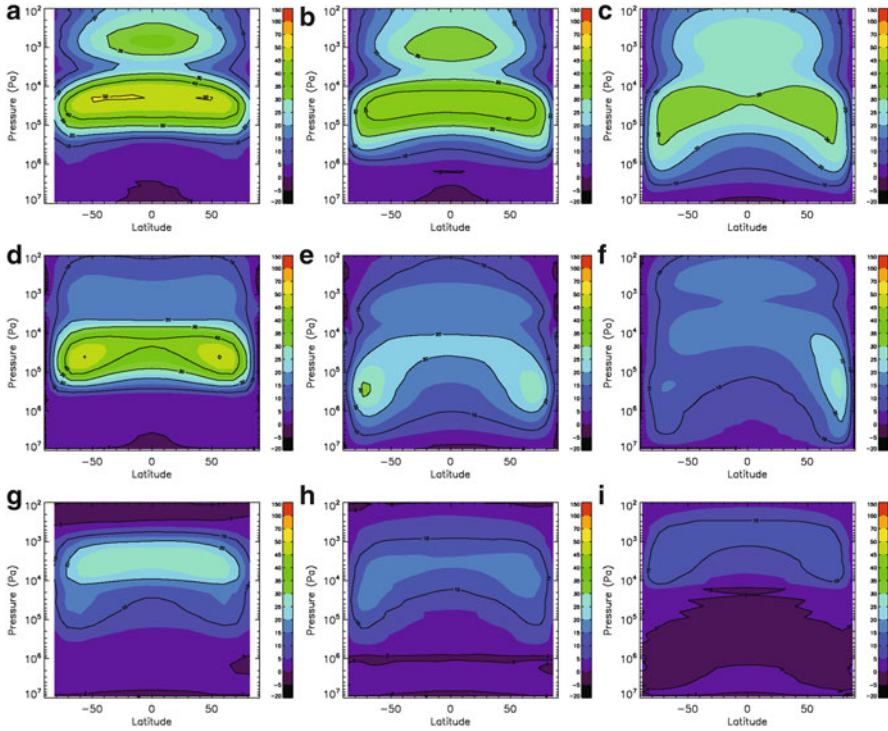


Fig. 8.9 Zonally and temporally averaged zonal winds obtained when varying the horizontal resolution. First row corresponds to the CCSR model, second row to the LMD model and third row to the OU model. First column is the low resolution simulations, middle column is the base runs and third column is the high resolution simulations

8.3.4.5 Horizontal Resolution

The effect of horizontal resolution is quite significant for all the models presented in Figs. 8.9 and 8.10. For both the CCSR and the LMD models, increasing the resolution tends to diminish the peak zonal wind in the 10^5 – 10^4 Pa pressure range and to increase the deep atmosphere winds over the poles. Though the amplitude and shape of the zonal wind field are not exactly similar between both models, these trends appear to be consistent.

In the case of the OU model, the evolution of the peak zonal wind with the resolution follows the same trend—amplitude decreases when resolution increases. However, the shift of higher winds towards the deep polar regions is not seen in this case.

Due to the high resolution used for the UCLA model, it should also be discussed by comparison to the *hres* simulations. However, comparison between Figs. 8.9 and 8.2h indicates more correspondence between the UCLA simulation and the *hres* simulations rather than with the *hres* simulations. Again, keep in mind that the

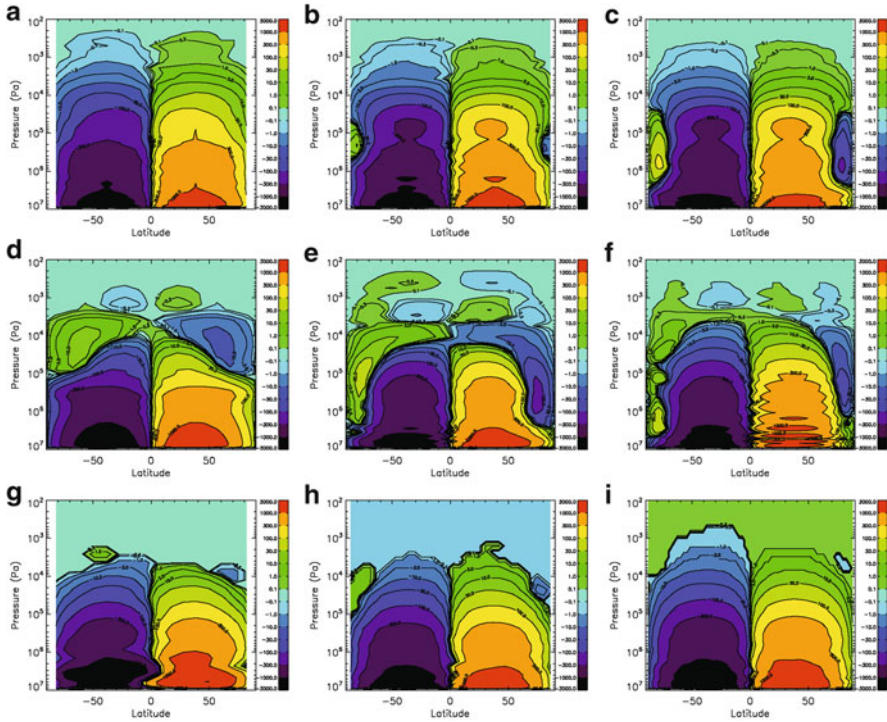


Fig. 8.10 Zonally and temporally averaged stream functions obtained when varying the horizontal resolution. First row corresponds to the CCSR model, second row to the LMD model and third row to the OU model. First column is the low resolution simulations, middle column is the base runs and third column is the high resolution simulations

results of the UCLA run are averaged over a 10-year period. Unfortunately, the impact of the resolution could not be tested with this model.

Changing the resolution clearly affects the zonal wind distributions, even if a consistent trend may not be found for all the models. It also affects the meridional cells, with the development of a much deeper reverse cell over the poles, as seen in Fig. 8.10. The polar regions appear to be very sensitive to the resolution, as well as the amplitude of the zonal winds in the cloud region. The connection between both effects is certainly done through the angular momentum transport budget.

8.3.4.6 Different Initial States

When the zonal wind is initialized with a pre-defined super-rotating field, the initial total angular momentum is high (around 15 times the angular momentum at rest, for the chosen wind distribution). It decreases with time, but the level at which it stabilizes depends on the model, as for the baseline case. The final zonal wind and

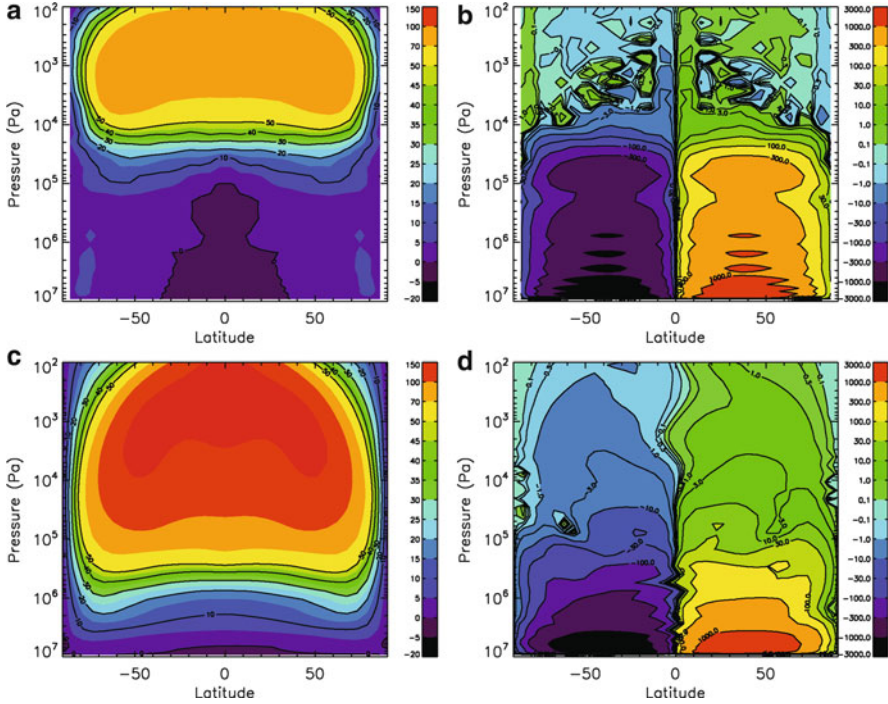


Fig. 8.11 Zonally and temporally averaged zonal wind and stream function obtained in the simulations with modified initial conditions (zonal wind already in super-rotation, *uini*): (a, b) CCSR model and (c, d) LMD model

stream function fields for the two models that tested this case (CCSR and LMD) are displayed in Fig. 8.11.

In both simulations, the zonal wind maximum is much higher than in the baseline case. However, the shape of the wind distribution is different in each model. In the CCSR-*uini* simulation, the wind below 10^5 Pa becomes very small, with a region of retrograde winds around the equator, reaching as high as 10^5 Pa. This explains why the total angular momentum goes down to 1.3, even lower than in the baseline simulation (Fig. 8.1). In the case of the LMD model, this region of negative values for u is also present, but confined to the near surface, and the deep atmospheric zonal wind is still comparable to observations. The total angular momentum is then high (factor around 6), though it has not yet reached an equilibrium after the 350 Venus days of the simulation. This simulation looks very similar to the LMD-pbl3 run.

The sensitivity to initial conditions in simulations of super-rotating atmospheres has been previously studied by Del Genio and Zhou (1996) and Kido and Wakata (2008). In the experiments reported in Del Genio and Zhou (1996), the rotation rate of the simulated planet varied, to test the sensitivity to this parameter, but the influence of initial conditions was also tested in the case of Titan-like and Venus-like rotation rate. In both cases, the same equilibrium was reached when starting

from rest or from strong zonal winds. Comparing to previous experiments (Del Genio et al. 1993), where different initial states lead to a different equilibrium in a Venus-like simulation, the authors conclude that the change from single- to double-precision computation may explain the results, due to a better angular momentum conservation.

Using a model based on the CCSR-NIES GCM, Kido and Wakata (2008) explored the impact of initial conditions on the resulting simulations of Venus zonal winds. When starting from rest, the zonal winds obtained show two high-latitude jets with peak values around 60 m/s, a distribution quite similar to the LR10-s baseline simulation (Fig. 8.2e). When starting from an atmosphere already in super-rotation, the wind field appears qualitatively similar, but the jets reach peak zonal winds up to 120 m/s. These two different final states indicate a similar behavior for this model, compared to the behavior obtained in our intercomparison work.

The angular momentum conservation has been checked in baseline configurations for the different models presented here. However, the question of detailed angular momentum budget in the simulations started from an artificially super-rotating state may be investigated further, in order to evaluate the impact of this conservation on the obtained multiple stable states.

8.4 Discussion

We have discussed here several series of simulations obtained by different models but with an effort to equalize the physical forcing and parametrization. The dispersion of the results is quite surprising, but may help to understand the directions where progress is needed in atmospheric modeling, at least in the case of the atmosphere of Venus. Other works have been published previously on GCM simulations of the atmosphere of Venus. They have been described in the previous chapter of this book. Though these simulations were not obtained under similar conditions as those in this present work, some results have been discussed in the previous section. It is also to be noted that many of these simulations show wind fields that fit within the dispersion obtained here. As an example, the wind field displayed in Fig. 8.4 of Del Genio and Zhou (1996), obtained for an Earth-like planet rotating as slowly as Venus, presents similarities (wind amplitude, shape of high-latitude jets) with those of Fig. 8.2.

In most cases, the amplitude and shape of the zonal wind field obtained with these models, though the atmosphere is in super-rotation, may not be exactly comparable to the observations of the latitudinal profile of zonal wind at the cloud-top level (Sanchez-Lavega et al. 2008), or of the vertical profiles of the zonal winds obtained with probes. One point noticed many times before is that to obtain zonal wind peaks around 100 m/s, it is often needed, when using simple radiative forcing, to induce an unrealistically high latitudinal contrast in the deep atmosphere.

How may modelers improve this comparison? Based on the work by Lebonnois et al. (2010), it appears that the radiative forcing chosen does have a strong effect

on the meridional circulation, and therefore on the angular momentum transport in the atmosphere. However, the intercomparison done in the present work clearly indicates that the modeled circulation is highly sensitive to many aspects of the models. In particular, the polar regions and the way they are treated in each model may be responsible for the different behaviors described here.

8.4.1 Simplified Radiative Forcing: Implications

The use of a simplified parametrization for the radiative forcing has a strong impact on the meridional circulation. The circulation obtained in all the previous works using such a parametrization consists of two large Hadley cells, with ascending motion in the equatorial region, poleward motions almost everywhere in the atmosphere, descending motions over each poles, and the returning equator-ward branch very close to the surface. In addition, a reverse cell is sometimes seen over the polar region, in and above the cloud region though it may go deeper in some cases.

In the case of a realistic radiative forcing, as discussed in [Lebonnois et al. \(2010\)](#), the circulation shows a pattern with more layers. The dominant Hadley-type cells are present in the cloud region, with a returning branch below the clouds, and a second set of cells in the deep atmosphere. This circulation is quite different from the circulation obtained with simplified forcing, and therefore it induces a global angular momentum transport pattern that must also be quite different. In the simulation presented in [Lebonnois et al. \(2010\)](#), high zonal winds peaking at roughly 60 m/s are present only in and above the clouds, with a significant role for the thermal tides in the concentration of angular momentum over equatorial regions. The effect of the diurnal cycle, with three-dimensional solar heating, should also be considered in the models with simplified forcing, to investigate the thermal tides.

Therefore, it is clear that the simplified radiative forcing affects the overall circulation significantly. As the radiative modeling suggests, the simplified forcing misses the significant cooling within the cloud deck, and probably overestimates (or incorrectly attributes) the heating in the lower atmosphere. To what extent can the sensitivity results of this intercomparison study be extrapolated to other radiative forcing simulations? The answer to this question is far from obvious. However, with more models using new radiative transfer forcings, the sensitivity of the results to modeling choices will certainly need to be evaluated.

8.4.2 Role of Polar Regions

The polar regions may represent a significant source of differences between the different dynamical cores, e.g., due to the filters used in finite different schemes. The sensitivity tests done with varying resolutions have shown that the zonal wind

field variations were correlated with variations of the stream function over the polar regions. Formations of jets and indirect circulations in the polar regions are clearly sensitive to the horizontal resolutions. The transport of angular momentum in these regions may be a key element to investigate in order to better understand these differences. These investigations have not been possible during this intercomparison campaign, but it should be a goal for future work.

8.4.3 Key Questions, Recommendations

The work we have conducted with these different GCMs illustrate how difficult it is to reproduce the same angular momentum budget and balance with different models, even when most parameterizations are chosen to be identical. This angular momentum balance is extremely sensitive to many model parameters, whether in the dynamical core or in the physical parameterizations. It is also quite complex to build tools accurate enough to investigate details of this budget, to explore how variations on one or the other parameter does affect the overall balance. It would certainly be an interesting direction to explore for future coordinated investigations: build an intercomparison protocol oriented towards angular momentum budget, transport terms and balance. Such detailed studies would also help to quantify and verify angular momentum conservation, which should affect the overall balance of momentum and therefore the meridional and zonal circulations.

Among the most sensitive parameters, this work points out the topography, the planetary boundary layer scheme, and the vertical and horizontal resolutions. Though its role is not obvious from the present work, the topography is certainly affecting the meridional circulation, as well as the budget of angular momentum. Concerning the boundary layer, the LMD-pb13 simulation may indicate a more efficient upward transport, allowing the atmosphere to transfer quickly angular momentum into the cloud region, and therefore reaching a similar state as when started with an excess of angular momentum (*uini* simulation). For the boundary layer, but also for other aspects such as atmospheric turbulence and convection, or the role of gravity waves, parametrization of subgrid-scale physical processes (meso/micro-scale dynamics of waves and turbulence) is a significant direction for further research in Venus general circulation modeling.

The choice of vertical and horizontal resolutions does affect the results. This is a difficult aspect of the problem, since we are limited by computer power. Therefore, the zonal and meridional wind strength should always be considered with caution until this dependence may be waived. In the case of the vertical resolution, there may be regions where the resolution should be improved, while in other regions this dependence is less significant. This analysis is certainly a study that needs to be done in the near future.

The sensitivity of the circulation to the initial state raises questions. Is this due to very long timescales to reach a completely steady state? Is it related to angular

momentum conservation? Are there other processes to be taken into account that would help solve this problem (such as gravity waves)? These questions need to be addressed by further modeling efforts.

This intercomparison work should be persuade in the future. It should include a quantitative assessment of the angular momentum budget, transport terms and balance, as well as the analysis of waves and their role in the transport of angular momentum. It would also be very interesting work to do when several improved models with realistic radiative transfer modules will be mature.

Acknowledgements SL would like to thank the Centre National d'Etudes Spatiales (CNES), the project Exoclimats financed by the Agence Nationale de la Recherche (ANR), and the computation facilities of both the Institut du Développement et des Ressources en Informatique Scientifique (IDRIS) and the University Pierre and Marie Curie (UPMC). The LR10 simulations were performed on Caltech's Division of Geological & Planetary Sciences Dell cluster, CITerra, funded by a grant from NASA under the Planetary Atmospheres program. MY conducted the numerical experiments at the Information Technology Center of the University of Tokyo and the Information Initiative Center of Hokkaido University, which were supported by Grant-in-Aid for Scientific Research (KAKENHI No. 20740273 and 22244060). HFP and GS acknowledge support from NASA's Planetary Atmospheres Program through Grant NASA NNX07AF27G.

References

- A.D. Del Genio, W. Zhou, Simulations of superrotation on slowly rotating planets: Sensitivity to rotation and initial condition. *Icarus* **120**, 332–343 (1996), doi:10.1006/icar.1996.0054
- A.D. Del Genio, W. Zhou, T.P. Eichler, Equatorial superrotation in a slowly rotating GCM - implications for Titan and Venus. *Icarus* **101**, 1–17 (1993), doi:10.1006/icar.1993.1001
- T.E. Dowling, M.E. Bradley, E. Colon, J. Kramer, R.P. LeBeau, G.C.H. Lee, T.I. Mattox, R. Morales-Juberias, C.J. Palotai, V.K. Parimi, A.P. Showman, The EPIC atmospheric model with an isentropic/terrain-following hybrid vertical coordinate. *Icarus* **182**, 259–273 (2006)
- A. HerrNSTein, T.E. Dowling, Effects of topography on the spin-up of a Venus atmospheric model. *J. Geophys. Res.-Planets* **112**, 4 (2007), doi:10.1029/2006JE002804
- J.L. Hollingsworth, R.E. Young, G. Schubert, C. Covey, A.S. Grossman, A simple-physics global circulation model for Venus: Sensitivity assessments of atmospheric superrotation. *Geophys. Res. Lett.* **34**, 5202 (2007), doi:10.1029/2006GL028567
- F. Hourdin, F. Couvreur, L. Menut, Parameterization of the dry convective boundary layer based on a mass flux representation of thermals. *J. Atmos. Sci.* **59**, 1105–1123 (2002)
- A. Kido, Y. Wakata, Multiple equilibrium states appearing in a Venus-like atmospheric general circulation model. *J. Meteorol. Soc. Japan* **86**, 969–979 (2008)
- S. Lebonnois, F. Hourdin, V. Eymet, A. Crespin, R. Fournier, F. Forget, Superrotation of Venus' atmosphere analyzed with a full general circulation model. *J. Geophys. Res.-Planets* **115**, 6006 (2010), doi:10.1029/2009JE003458
- C. Lee, Modelling of the atmosphere of Venus, Ph.D. thesis, University of Oxford (2006)
- C. Lee, M.I. Richardson, A general circulation model ensemble study of the atmospheric circulation of venus. *J. Geophys. Res. Planets* **115**, E04002 (2010), doi:10.1029/2009JE003490
- C. Lee, S.R. Lewis, P.L. Read, A numerical model of the atmosphere of Venus. *Adv. Space Res.* **36**, 2142–2145 (2005), doi:10.1016/j.asr.2005.03.120
- C. Lee, S.R. Lewis, P.L. Read, Super-rotation in a venus general circulation model. *J. Geophys. Res. Planets* **112**, L04204 (2007), doi:10.1029/2006JE002874

- G.L. Mellor, T. Yamada, Development of a turbulent closure model for geophysical fluid problems. *Rev. Geophys. Space Phys.* **20**, 851–875 (1982)
- A.S. Monin, A.M. Obukhov, Basic laws of turbulent mixing in the ground layer of the atmosphere. *Trans. Geophys. Inst. Akad. Nuak.* **151**, 1963–1987 (1954)
- M. Newman, C.B. Leovy, Maintenance of strong rotational winds in Venus' middle atmosphere by thermal tides. *Science* **257**, 647–650 (1992)
- H.F. Parish, G. Schubert, C. Covey, R.L. Walterscheid, A. Grossman, S. Lebonnois, Decadal variations in a Venus General Circulation Model. *Icarus*, **212**, 1, 42–65, doi:10.1016/j.icarus.2011.11.015, 2011 accepted (2011)
- P. Read, Super-rotation and diffusion of axial angular momentum : II. a review of quasi-axisymmetric models of planetary atmospheres. *Quater. J. R. Met. Soc.* **112**, 253–272 (1986)
- A. Sanchez-Lavega, R. Hueso, G. Piccioni, P. Drossart, J. Peralta, S. Perez-Hoyos, C.F. Wilson, F.W. Taylor, K.H. Baines, D. Luz, S. Erard, S. Lebonnois, Variable winds on Venus mapped in three dimensions. *Geophys. Res. Lett.* **35**, L13204 (2008)
- A. Seiff, J.T. Schofield, A.J. Kliore, F.W. Taylor, S.S. Limaye, H.E. Revercomb, L.A. Sromovsky, V.V. Kerzhanovich, V.I. Moroz, M.Y. Marov, Models of the structure of the atmosphere of Venus from the surface to 100 kilometers altitude. *Adv. Space Res.* **5**(11), 3–58 (1985)
- M. Takagi, Y. Matsuda, Effects of thermal tides on the Venus atmospheric superrotation. *J. Geophys. Res.-Atmos.* **112**, 9112 (2007), doi:10.1029/2006JD007901
- M. Yamamoto, M. Takahashi, The fully developed superrotation simulated by a General Circulation Model of a Venus-like atmosphere. *J. Atmos. Sci.* **60**, 561–574 (2003a), doi:10.1175/1520-0469(2003)060
- M. Yamamoto, M. Takahashi, Superrotation and equatorial waves in a T21 Venus-like AGCM. *Geophys. Res. Lett.* **30**, 090 000–1 (2003b), doi:10.1029/2003GL016924
- M. Yamamoto, M. Takahashi, Dynamics of Venus' superrotation: The eddy momentum transport processes newly found in a GCM. *Geophys. Res. Lett.* **31**, 9701 (2004), doi:10.1029/2004GL019518
- M. Yamamoto, M. Takahashi, Superrotation maintained by meridional circulation and waves in a Venus-like AGCM. *J. Atmos. Sci.* **63**, 3296–3314 (2006), doi:10.1175/JAS3859.1
- M. Yamamoto, M. Takahashi, Dynamical effects of solar heating below the cloud layer in a Venus-like atmosphere. *J. Geophys. Res.* **114**, E12004 (2009), doi:10.1029/2009JE003381
- R.E. Young, J.B. Pollack, A three-dimensional model of dynamical processes in the Venus atmosphere. *J. Atmos. Sci.* **34**, 1315–1351 (1977), doi:10.1175/1520-0469(1977)034